Earth and Planetary Science Letters 450 (2016) 306–316

Contents lists available at ScienceDirect

Earth and Planetary Science Letters

www.elsevier.com/locate/epsl

Middle to Late Pleistocene vegetation and climate change in subtropical southern East Africa

Isla S. Castañeda [a,b,*], Thibaut Caley [c,d], Lydie Dupont [e], Jung-Hyun Kim [a,f], Bruno Malaizé [c], Stefan Schouten [a]

[a] NIOZ Royal Netherlands Institute for Sea Research, Department of Marine Microbiology and Biogeochemistry, and Utrecht University, PO Box 59, 1790 AB Den Burg, The Netherlands
[b] University of Massachusetts Amherst, Department of Geosciences, 611 N Pleasant St., 233 Morrill Science Center II, Amherst, MA 01003, USA
[c] CRNS, EPOC, UMR 5805, Université de Bordeaux, Allée Geoffroy St Hilaire, 33615 Pessac, France
[d] IFREMER, Laboratoire Environnements Sédimentaires, BP70, 29280 Plouzané, France
[e] MARUM Center for Marine Environmental Sciences, University of Bremen, Germany
[f] Department of Marine Science and Convergence Technology, Hanyang University ERICA Campus, 55 Hanyangdaehak-ro, Sangnok-gu, Ansan-si, Gyeonggi-do 426-791, South Korea

ARTICLE INFO

Article history:
Received 24 January 2016
Received in revised form 23 June 2016
Accepted 26 June 2016
Available online xxxx
Editor: M. Frank

Keywords:
vegetation
Africa
n-alkane
pollen
Subtropical Front
Mid-Brunhes

ABSTRACT

In this study we investigate Pleistocene vegetation and climate change in southern East Africa by examining plant leaf waxes in a marine sediment core that receives terrestrial runoff from the Limpopo River. The plant leaf wax records are compared to a multi-proxy sea surface temperature (SST) record and pollen assemblage data from the same site. We find that Indian Ocean SST variability, driven by high-latitude obliquity, exerted a strong control on the vegetation of southern East Africa during the past 800,000 yr. Interglacial periods were characterized by relatively wetter and warmer conditions, increased contributions of C_3 vegetation, and higher SST, whereas glacial periods were marked by cooler and arid conditions, increased contributions of C_4 vegetation, and lower SST. We find that Marine Isotope Stages (MIS) 5e, 11c, 15e and 7a–7c are strongly expressed in the plant leaf wax records but MIS 7e is absent while MIS 9 is rather weak. Our plant leaf wax records also record the climate transition associated with the Mid-Brunhes Event (MBE) suggesting that the pre-MBE interval (430–800 ka) was characterized by higher inputs from grasses in comparison to relatively higher inputs from trees in the post-MBE interval (430 to 0 ka). Differences in vegetation and SST of southern East Africa between the pre- and post-MBE intervals appear to be related to shifts in the location of the Subtropical Front. Comparison with vegetation records from tropical East Africa indicates that the vegetation of southern East Africa, while exhibiting glacial–interglacial variability and notable differences between the pre- and post-MBE portions of the record, likely did not experience such dramatic extremes as occurred to the north at Lake Malawi.

1. Introduction

The Earth experienced numerous fluctuations between cold glacial periods and warm interglacial periods during the Pleistocene. Individual glacial and interglacial periods were characterized by varying boundary conditions including insolation, continental ice sheet extent and atmospheric carbon dioxide (pCO_2) concentrations, resulting in differing intensities and associated patterns of climate variability (Past Interglacials Working Group of PAGES, 2016). Accompanying glacial–interglacial variability, long-term climate transitions also occurred. During the mid-Pleistocene transition (1.2–0.6 Ma), variations in global ice volume shifted from exhibiting a dominant 41 kyr periodicity to a 100 kyr periodicity and a number of atmospheric and oceanic circulation changes took place (Past Interglacials Working Group of PAGES, 2016). Another climate transition, the Mid-Brunhes Event (MBE), placed between Marine Isotope Stages (MIS) 12/11 at 430 ka, marks an increase in the amplitude of glacial–interglacial cycles after this time (Jansen et al., 1986; EPICA Community Members, 2004).

On the African continent dramatic and rapid climate fluctuations frequently occurred during the Pleistocene, which are

* Corresponding author at: University of Massachusetts Amherst, Department of Geosciences, 611 N Pleasant St., 233 Morrill Science Center II, Amherst, MA 01003, USA.
E-mail address: isla@geo.umass.edu (I.S. Castañeda).

http://dx.doi.org/10.1016/j.epsl.2016.06.049
0012-821X/

thought to have contributed to major steps in human evolution and to the development of modern behavior (e.g. Compton, 2011; deMenocal, 2004; Trauth et al., 2009). Presently, continuous records of African continental climate spanning beyond the Last Glacial Maximum (MIS 2) are relatively rare. A number of Plio-Pleistocene marine records exist from the tropical and subtropical regions offshore northwest and northeast Africa (deMenocal, 2004) while numerous lakes and paleolakes of the East African Rift valley have provided both long, continuous records and brief snapshots into past climate during discrete intervals (e.g. Scholz et al., 2007; Cohen et al., 2007). These records reveal dramatic past hydroclimate and vegetation fluctuations as well as a high degree of spatial variability. In contrast, the subtropical southern African continent, a region that hosted early hominin species (e.g. Compton, 2011), remains understudied.

Here we examine plant leaf waxes from a marine sediment core to investigate vegetation change in southern East Africa during the past 800,000 yr. We compare our records to pollen (Dupont et al., 2011) and sea surface temperature (SST) (Caley et al., 2011) reconstructions from the same core. Pollen and plant macrofossils are commonly used to examine vegetation change, a sensitive indicator of past climate conditions. A complementary approach is to examine the distribution and isotopic composition of plant leaf waxes. High molecular weight *n*-alkanes (29 to 33 carbon atoms) are a main component of plant epicuticular waxes (Eglinton and Hamilton, 1967). The distribution of dominant homologues can reflect environmental conditions while the carbon isotopic composition ($\delta^{13}C$) of *n*-alkanes provides information on the dominant photosynthetic pathway (C_3 or C_4) used (Collister et al., 1994). Our records provide insights into the role of Indian Ocean SST and orbital forcing in driving subtropical vegetation change.

2. Study location and methods

2.1. Study location

Giant piston core MD96-2048 (37.59 m, 660 m depth), located in the precursor region of the Agulhas Current, was retrieved by the R/V Marion Dufresne during the 104 MOZAPHARE cruise from the upper continental slope offshore Mozambique, south of the Limpopo River mouth (26°10′S, 34°01′E) (Fig. 1). The uppermost 12 m of the core, spanning the past 800 ka, is examined. The age model was previously published by Caley et al. (2011) and is based on oxygen isotope stratigraphy. Pollen and spore analysis of the upper part of the core (MIS 9 to 1) is reported by Dupont et al. (2011). The SST record is based on a stacked record of the $U^{K'}_{37}$ Index, the TEX_{86} paleothermometer and Mg/Ca ratios of *G. ruber s.s.* (Caley et al., 2011).

The Limpopo River is the second largest African river draining into the Indian Ocean after the Zambezi River. Its watershed includes parts of Botswana, Zimbabwe, southern Mozambique and northern South Africa (Fig. 1). Watershed elevation varies greatly ranging from lowland coastal regions to >2000 m on the interior central southern Africa plateau. Mean annual temperature and precipitation ranges from 16 °C and 1400 mm in the central plateau region to 24 °C and 600 mm in the lowlands (Dupont et al., 2011). Presently, a strong relationship exists between southwest (SW) Indian Ocean SST and southern East African precipitation. Most rainfall occurs in austral summer (November to March) with precipitation increasing in late summer when SW Indian Ocean SSTs are the highest (Jury et al., 1993; Reason and Mulenga, 1999). The vegetation of the Limpopo catchment is highly variable and includes closed forest, dry scrubland, alpine open grasslands and semi-evergreen lowland forest (Fig. 1; White, 1983). For a detailed description of modern vegetation in the Limpopo catchment the reader is referred to Dupont et al. (2011).

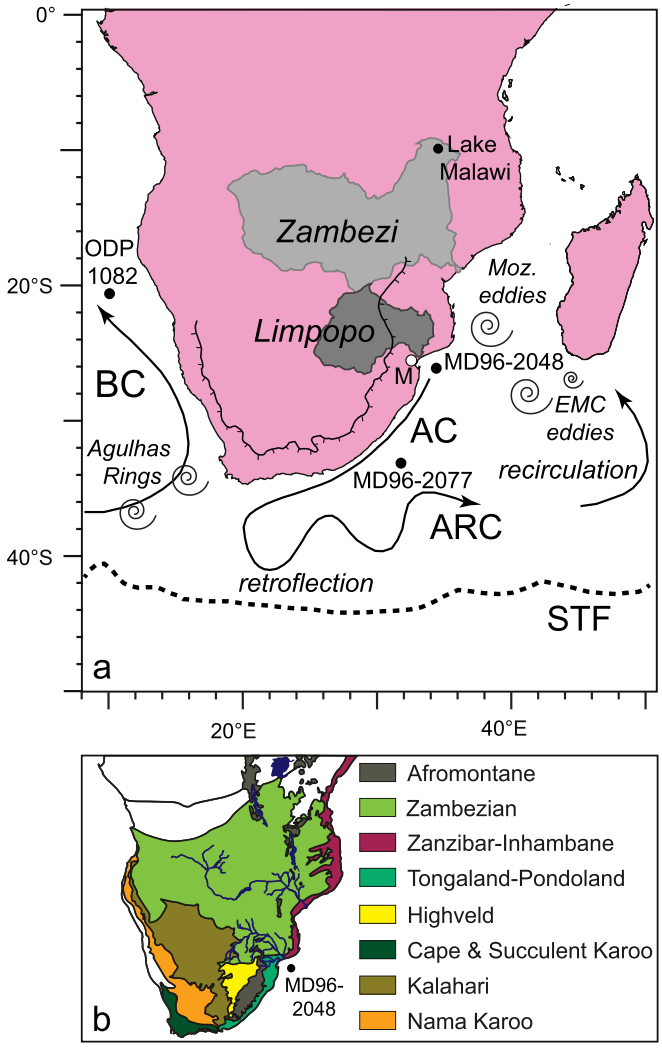

Fig. 1. Map of the southern African continent with core locations and major surface currents drawn based on Caley et al. (2011). The locations of marine cores MD96-2048 (this study), MD96-2077 (Bard and Rickaby, 2009) and ODP Site 1082 (Jahn et al., 2003) are shown. The Zambezi and Limpopo River basins are outlined by the light and dark gray shading, respectively. The black line drawn on southern region of the continent indicates the location of the Great Escarpment. The location of Maputo (M) is given by the white dot and the approximate location of drill core MAL05-1c from Lake Malawi is indicated (Scholz et al., 2007; Cohen et al., 2007; Beuning et al., 2011). The Agulhas Current (AC), Agulhas Return Current (ARC), Benguela Current (BC) are the major surface currents in the region and are shown by the labeled arrows. Sites of retroflection and recirculation are noted. The approximate location of eddies of the Mozambique Channel (Moz.), East Madagascar Current, and the Agulhas Rings, which transport heat and salt into the Atlantic Ocean, are indicated. The dashed line indicates the location of the Subtropical Front (STF). b) The plant geographical regions of southern Africa (figure modified from Dupont et al., 2011, which is based on White, 1983). The five regions relevant for our study are Zambezian (tropical, mainly savanna and woodland), Zanzibar–Inhambane (tropical, mainly forest), Highveld (subtropical grassland), Tongaland–Pondoland (subtropical forest) and Afromontane (White, 1983).

2.2. Organic geochemical analyses

177 samples from core MD96-2048 were freeze dried and extracted with an Accelerated Solvent Extractor (ASE 200) using a mixture of 9:1 dichloromethane (DCM) to methanol (MeOH). Samples were separated into apolar, ketone and polar fractions with alumina oxide using solvent mixtures of 9:1 (vol:vol) hexane/DCM, 1:1 (vol:vol) hexane/DCM, and 1:1 (vol:vol) DCM/MeOH, respectively. The apolar fractions were passed through Ag^+ impregnated silica to separate saturated and unsaturated hydrocarbons.

Identification of *n*-alkanes was performed on a Thermo Finnigan Trace Gas Chromatograph (GC) Ultra coupled to Thermo Finnigan DSQ mass spectrometer (MS) using a CP Sil-5 fused silica capillary column (25 m × 0.32 mm; film thickness 0.12 μm) with helium as the carrier gas. Mass scans were made from $m/z =$ 50 to 800 with 3 scans per second and an ionization energy of 70 eV. The oven program initiated at 70 °C, increased by a rate of 20 °C min^{-1} to 130 °C, and subsequently by a rate of 4 °C min^{-1} until 320 °C (held for 10 min).

Quantification of *n*-alkanes was performed on an HP 6890 gas chromatograph (GC) using a 50 m CP Sil-5 column (0.32 mm diameter, film thickness 0.12 μm), helium as the carrier gas, and the same oven program as for GC-MS. Compound concentrations were determined by relating chromatogram peak areas to the concentration of an internal standard of known concentration. The average chain length (ACL; Poynter et al., 1989) was calculated using the C_{27} to C_{33} *n*-alkanes (many samples did not contain shorter homologues):

$$ACL = \frac{27C_{27} + 29C_{29} + 31C_{31} + 33C_{33}}{(C_{27} + C_{29} + C_{31} + C_{33})},$$

where C_x represents the abundance of the *n*-alkane with *x* carbon atoms.

Compound-specific $\delta^{13}C$ analyses were performed on the aliphatic fraction using an Agilent 6800 GC coupled to a ThermoFisher Delta V isotope ratio monitoring mass spectrometer. Isotope values were measured against a calibrated external reference gas and instrument performance was monitored by daily injection of a mixture of C_{20} and C_{24} perdeuterated *n*-alkanes with known isotopic compositions. Squalane added as an internal standard to each sample provided an additional check on instrument performance. The $\delta^{13}C$ values for individual compounds are reported in the standard delta notation against the Vienna Pee Dee Belemnite (VPDB) standard. Ninety nine samples were analyzed in duplicate to quadruplicate with a reproducibility of on average ±0.36‰ for the C_{31} *n*-alkane.

3. Results

Concentrations of total long-chain *n*-alkanes (C_{27}–C_{33}) vary from 0.02 to 0.82 μg g sed^{-1} with a mean value of 0.27 μg g sed^{-1}. In general, concentrations and mass accumulation rates (MAR) of *n*-alkanes do not exhibit clear glacial–interglacial patterns with a few exceptions (Fig. 2). The lowest *n*-alkane concentrations and MARs are noted from ~491 to 522 ka during MIS 13. Elevated *n*-alkanes concentrations and MARs are noted during the MIS 2 and also in the older part of the core (526–620 ka and 680–800 ka). ACL ranges from 30.7 to 31.4 with a mean value of 30.9. Mean pre- and post-MBE (see section 4.5) ACL values are 31.0 and 30.9, respectively (Fig. 2).

The C_{29}–C_{33} *n*-alkanes were generally present in suitable concentrations to analyze their carbon isotopic composition. Here we report the carbon isotope composition of the C_{31} *n*-alkane (hereafter $\delta^{13}C_{wax}$, $n = 166$), the most abundant homologue. The C_{33} *n*-alkane was also abundant but it co-eluted with another compound so its isotopic composition could not be reliably measured. In core MD96-2048, $\delta^{13}C_{wax}$ values range from −23.8 to −27.9‰ (Fig. 2), with a mean value of −25.5‰. The $\delta^{13}C_{wax}$ record indicates generally lower values during interglacials and higher values during glacials. The average $\delta^{13}C_{wax}$ values in the pre-MBE and post-MBE intervals are similar at −25.6‰ and −25.4‰, respectively. The uppermost sample analyzed from MD96-2048 (0.36 ka) has a $\delta^{13}C_{wax}$ value of −25.8‰, similar to core top samples collected from 23–28°S from the Atlantic Ocean offshore western Namibia and South Africa, which vary from −25.2‰ to −26.1‰ (Vogts et al., 2012).

4. Discussion

4.1. Sources of n-alkanes

Plant leaf waxes are widely recognized as a resistant compound class and are known to be transported long-distances within large river systems (e.g. Ponton et al., 2014). Many previous studies have examined marine sediment cores situated in front of large river basins including the Nile (e.g. Castañeda et al., 2016), the Congo (e.g. Schefuß et al., 2003) and the Zambezi (e.g. Schefuß et al., 2011) to investigate basin-scale continental vegetation or hydroclimate change from leaf waxes, the approach we take here. A study of leaf wax hydrogen isotopes in Amazon River particulate organic matter, designed to test whether biomarkers present in rivers are representative of their catchment, concluded that leaf waxes in transit largely reflect catchment-averaged precipitation, thereby supporting this approach to paleoclimate reconstruction (Ponton et al., 2014).

Before inferring the vegetation and climatic history based on plant leaf waxes or pollen, the source area(s) of the vegetation must be determined. Plant leaf waxes are transported to marine sediments via wind or water erosion. Here, transport by the Limpopo River is likely the main transport mechanism as the dominant wind patterns do not facilitate transport of *n*-alkanes from the continent to the SW Indian Ocean because the surface airflow persists in an east–west (ocean to land) direction during most of the year (Tyson and Preston-Whyte, 2000). The coring site is also located close (within 120 km) to the mouth of the Limpopo River (Fig. 1). Furthermore, we note a significant positive correlation ($r^2 = 0.77$, $p < 0.001$) between mass accumulation rates (MAR) of total *n*-alkanes and total branched glycerol dialkyl glycerol tetraethers (brGDGTs) (Fig. 2). BrGDGTs are commonly found in soils (Weijers et al., 2007) and their presence at site MD96-2048 is attributed to Limpopo River runoff (Caley et al., 2011). Although overall terrestrial inputs to the coring site are low, as evidenced by low concentrations of *n*-alkanes, brGDGTs (Caley et al., 2011), and pollen grains (Dupont et al., 2011), the general agreement between brGDGT and *n*-alkane MARs (Fig. 2) suggests that fluvial transport is the dominant delivery mechanism of leaf waxes to site MD96-2048. Dupont et al. (2011) also concluded that most of the pollen and spores at this site are fluvially transported.

Based on pollen, Dupont et al. (2011) suggested that the main source area of material to MD96-2048 is from the region north of Maputo, extending from the Drakensberg (the eastern portion of the Great Escarpment) in the west to the coastal plain in the east (Fig. 1). We assume that plant leaf waxes in the same sediment core derive from an identical region. It should be noted that the source area of material within the Limpopo River catchment may have shifted in the past between different sub-basins under different climate regimes, as has been documented for other large river catchments including the nearby Zambezi (Just et al., 2014; van der Lubbe et al., 2016). However, this issue cannot be assessed for MD96-2048 with the data presently available. We note that the Zambezi River likely does not represent a significant source of material to site MD96-2048. Marine cores collected in front of the Zambezi and Limpopo Rivers reveal qualitative differences between pollen assemblages, with pollen from the Limpopo site consistent with vegetation reflecting overall lower temperatures (Dupont et al., 2011 and references therein) as expected for the more southerly position of the Limpopo catchment. Furthermore, the core site is located in the southern Limpopo cone deposition center, which has accumulated sediments since the Late Miocene, its location restricted aerially by a counter-current (Martin, 1981). Sediment transport from the Zambezi River is northward over the shelf to the upper part of the deep sea canyon during interglacials whereas sediment is mainly discharged on the slope in front of

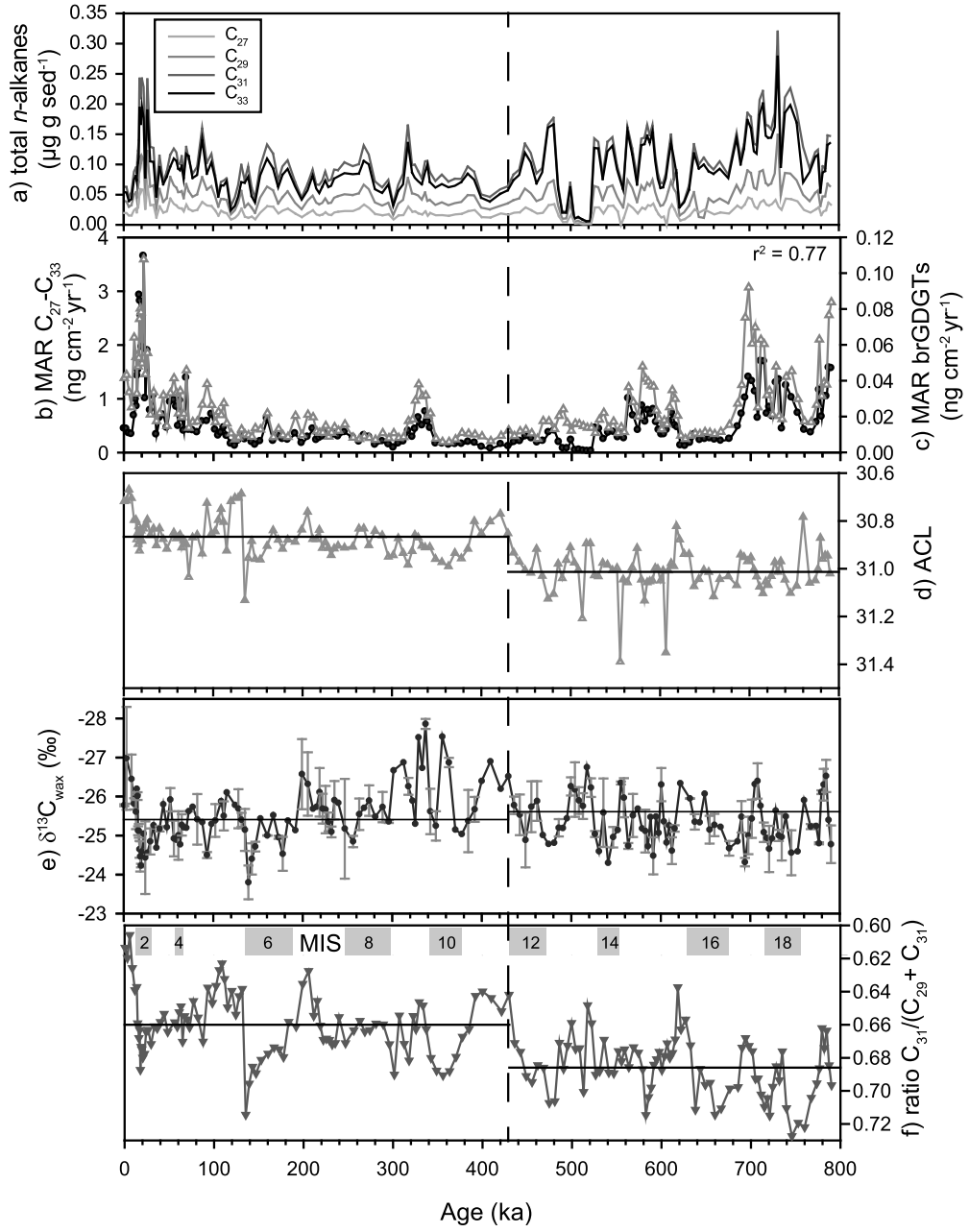

Fig. 2. MD96-2048 *n*-alkane data. a) The concentration of the nC_{27}, nC_{29}, nC_{31} and nC_{33} *n*-alkanes. The C_{31} *n*-alkane is the most abundant of the long-chain *n*-alkanes (mean concentration of 0.10 µg g sed^{-1}) followed by the C_{33} *n*-alkane (mean concentration of 0.09 µg g sed^{-1}) and the C_{29} *n*-alkane (mean concentration of 0.05 µg g sed^{-1}). b) The mass accumulation rate (MAR) of long-chain *n*-alkanes (sum of C_{27} to C_{33}; black circles) and c) the MAR of total branched glycerol dialkyl glycerol tetraethers (GDGTs; open gray triangles). d) The average chain length (ACL). e) The carbon isotopic composition of the C_{31} *n*-alkane ($\delta^{13}C_{wax}$). f) The $C_{31}/(C_{29}+C_{31})$ *n*-alkane ratio. In D, E and F the horizontal lines plot the mean values for the 800–430 ka and 430–0 ka intervals. The vertical dashed line at 430 ka indicates the MBE. The Marine Isotope Stages (MIS) are indicated by the numbers at the top of panel E.

the river mouth during sea level lowstands (Schulz et al., 2011; van der Lubbe et al., 2014). Therefore, it seems unlikely that Zambezi-derived material deposited at these locations could be displaced to the Limpopo cone (upper slope), over five degrees of latitude to the south.

4.2. Glacial–interglacial variability in plant leaf wax ratios

Several parameters based on the distribution of *n*-alkane homologues reflect environmental variability. For example, increasing ACL is observed with increasing aridity or temperature (e.g. Poynter et al., 1989; Rommerskirchen et al., 2003; Horikawa et al., 2010; Bush and McInerney, 2015). Likewise, the ratio of $C_{31}/(C_{29}+C_{31})$ *n*-alkanes is also used as a proxy for temperature or aridity (Horikawa et al., 2010). We focus leaf wax discussion on the $C_{31}/(C_{29}+C_{31})$ ratio, which most clearly resolves the glacial/interglacial cycles. This ratio likely reflects vegetation change on the African landscape as rainforest species dominantly produce the C_{29} *n*-alkane while savanna species (including trees, herbs and shrubs) dominantly produce the C_{31} *n*-alkane (Vogts et al., 2009).

The glacial–interglacial cycles of the past 800 ka are strongly expressed in the $C_{31}/(C_{29}+C_{31})$ ratio except for Termination III, marking the transition between MIS 8/7, which is not expressed in the *n*-alkane records (Fig. 3). While the interval of substages 7a through 7c is marked by a clear excursion to lower $C_{31}/(C_{29}+C_{31})$

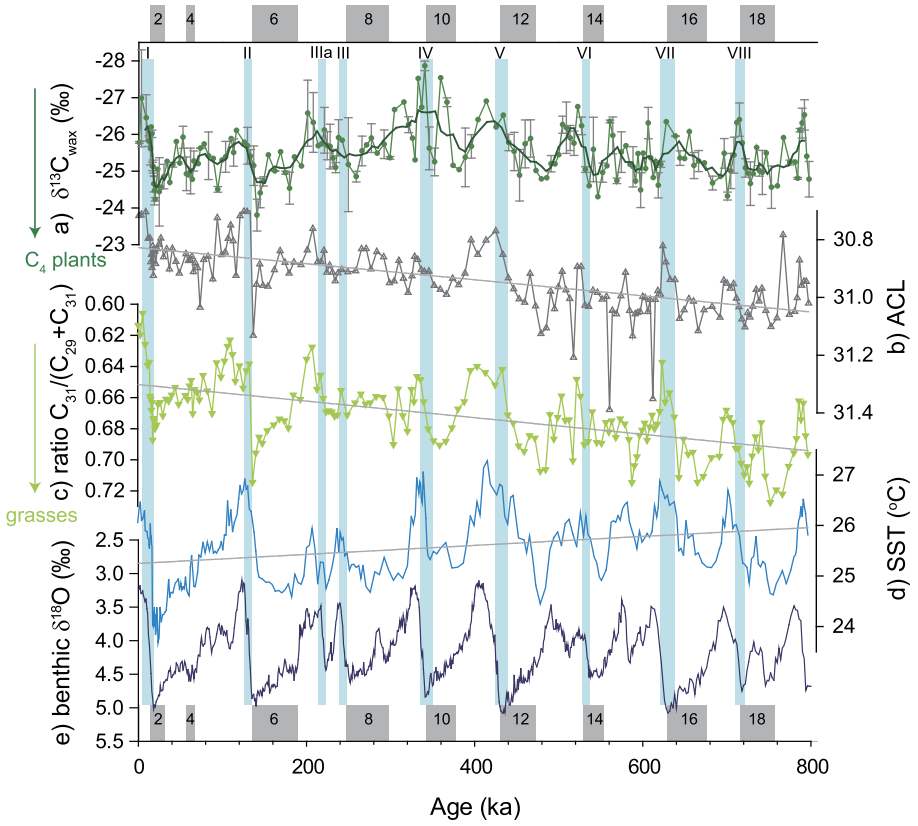

Fig. 3. Summary of paleoclimate records during the past 800 ka. a) The carbon isotopic composition of the C_{31} *n*-alkane ($\delta^{13}C_{wax}$). The thick green line represents the smoothed data (5 point running mean). Higher (less negative) values indicate increased inputs from C_4 vegetation. b) Average chain length (ACL). Higher ACL values occur at times of lower SST and thus are likely mainly reflecting changes in aridity. c) The $C_{31}/(C_{29}+C_{31})$ *n*-alkane ratio. Higher values suggest increased inputs of grasses (C_{31}) and likely reflect arid conditions. d) The SST record of core MD96-2048 based on the stacked record of the $U^{K'}_{37}$ Index, Mg/Ca ratios of *G. ruber s.s.*, and TEX_{86}. Data from Caley et al. (2011). In b, c, and d, the straight gray lines indicate the overall trend over the past 800 ka. e) The global benthic oxygen isotope ($\delta^{18}O$) stack is shown for comparison (Lisiecki and Raymo, 2005). Marine Isotope Stages (MIS) are indicated by the gray boxes and numbers at the bottom and top of the graph. The vertical blue bars and roman numerals at the top indicate glacial terminations. With the exception of SST (d), all *y*-axes are reversed. (For interpretation of the references to color in this figure legend, the reader is referred to the web version of this article.)

values, the absence of substage 7e, coupled with a weak MIS 8 glacial, results in the absence of Termination III. In agreement with our data, MIS 7 is recognized as a weak interglacial while the part of MIS 8 immediately before Termination III is a weak glacial at many sites (Lang and Wolff, 2011). MIS 7 is a particularly intriguing interglacial as substage 7e is the strongest signal at some locations whereas at others 7c is the strongest (Lang and Wolff, 2011). In other records, the entire interval of 7c through 7a appears as a rather strong interglacial (Lang and Wolff, 2011), which is the case for our vegetation records. Of the interglacials, MIS 11 and MIS 5 are recognized as the strongest of the past 800 ka with MIS 11 being exceptionally strong (Lang and Wolff, 2011). Both MIS 5e and 11c are clearly expressed in our leaf wax records, as is MIS 15e. Termination II, marking the transition from MIS 6/5, is particularly dramatic and abrupt in the $C_{31}/(C_{29}+C_{31})$ record (Fig. 3). Interestingly, while MIS 9 is recognized as a strong interglacial at many sites, including in the MD96-2048 SST record, it is relatively weak in the $C_{31}/(C_{29}+C_{31})$ record. Conversely, we also note that SW Indian Ocean SST was quite low during MIS 7a–c when a relatively strong response in the $C_{31}/(C_{29}+C_{31})$ record is detected. While the reasons for a weak expression of MIS 9 and a strong expression of 7a–c in our *n*-alkane records are not clear, likely other factors in addition to aridity, which in turn is related to SST variability, contributed to vegetation change at these times. Overall, the $C_{31}/(C_{29}+C_{31})$ record supports stronger glacial–interglacial vegetation variability in southern East Africa since the MBE (EPICA Community Members, 2004; Lang and Wolff, 2011).

Interestingly, a long term trend to lower ACL and $C_{31}/(C_{29}+C_{31})$ ratios occurs from 800 ka to the present. A long-term trend to lower SST also occurs over this interval (Fig. 3). While the SST trend is largely due to pronounced cooling during MIS 2, at ODP Site 1082, located offshore Namibia at 21.5°S, the opposite trend is observed where a long-term shift to lower oxygen isotope values of *Globorotalia inflata* reflects increasingly higher glacial SSTs toward the present (Jahn et al., 2003). This pattern may be related to long-term variability in the location of the Subtropical Front (STF), and the associated strength and position of the Agulhas Current and Agulhas Leakage (see section 4.5). However, the exact cause of the long term decrease in the $C_{31}/(C_{29}+C_{31})$ ratio remains unclear.

4.3. Leaf wax proxies and pollen

The stable carbon isotopic composition of plant leaf waxes ($\delta^{13}C_{wax}$) is used to distinguish vegetation utilizing the two major photosynthetic pathways. The C_3 pathway is the most common and is used by most trees, cold-season grasses and sedges while the C_4 pathway is utilized by warm season grasses and sedges and is common in tropical savannas. C_3 plants have lower carbon isotopic values in comparison to C_4 vegetation (Collister et al., 1994). For the C_{31} *n*-alkane, mean values of −35.2‰ and −21.7‰ are representative of C_3 and C_4 vegetation, respectively (Castañeda et al., 2009a). A third photosynthetic carbon-fixation pathway, the Crassulacean Acid Metabolism pathway, is typically used by a minor component of the vegetation and has isotopic values interme-

diate between those of C_3 and C_4 plants (Feakins and Sessions, 2010). Recent work indicates a larger variability in the range of C_3 plant carbon isotope values than previously thought (Diefendorf et al., 2010). However, C_3 vegetation is generally isotopically depleted in ^{13}C comparison to C_4 vegetation and thus $\delta^{13}C_{wax}$ can be used to examine relative inputs of C_3 vs. C_4 plants, although absolute values should be interpreted with care. A number of factors including temperature, aridity and pCO_2 can influence the distribution of C_3 and C_4 vegetation (e.g. Khon et al., 2014 and references therein). In tropical Africa previous studies have recognized aridity (precipitation) as the main factor controlling the continental scale distribution of C_3 vs. C_4 vegetation (e.g. Castañeda et al., 2009a; Schefuß et al., 2003) although more recent work suggests a greater influence of temperature and CO_2, particularly for glacial periods (Khon et al., 2014).

We find that ACL, the $C_{31}/(C_{29}+C_{31})$ ratio, and $\delta^{13}C_{wax}$ of MD96-2048 reveal similar overall trends (Fig. 3). Glacial periods are generally characterized by higher ACL values, higher $C_{31}/(C_{29}+C_{31})$ ratios and higher $\delta^{13}C_{wax}$ values. A study of the central USA found longer *n*-alkane chain lengths, and higher ACL values, were correlated with higher growing season temperature (Bush and McInerney, 2015). Likewise, to the north of the Limpopo basin at Lake Malawi, higher ACL values also are correlated with higher temperatures (Castañeda et al., 2009b). Conversely, in core MD96-2048 higher ACL values are noted during glacials, suggesting that temperature likely is not the dominant controlling factor on *n*-alkane chain length. Increased *n*-alkane chain lengths are also associated with increased aridity (Poynter et al., 1989; Schefuß et al., 2003). Thus in the Limpopo River drainage aridity or relative humidity is likely the main control on *n*-alkane chain length. The $\delta^{13}C_{wax}$ record indicates that glacial periods were also characterized by slightly higher contributions of C_4 vegetation (Fig. 3) although pollen data from the same core (Dupont et al., 2011) indicates that glacial–interglacial changes in the extent of grassy vegetation were not large. Dupont et al. (2011) infer that the combination of moderately less rainfall with lower temperatures drove the expansion of mountain vegetation during glacial periods.

To date a relatively limited number of studies have examined pollen and $\delta^{13}C_{wax}$ from the same samples (e.g. Huang et al., 2006; Rommerskirchen et al., 2006; Feakins, 2013; Hoetzel et al., 2013; Dupont et al., 2013). Plant leaf waxes provide complementary, but different, information on past vegetation assemblages in comparison to pollen. A fundamental difference is that *n*-alkanes are an indicator of biomass whereas pollen is a signal of reproduction (e.g. Hughen et al., 2004). Pollen can differentiate vegetation at the genus to species level whereas leaf wax distributions can provide insight into general plant life forms (e.g. trees or grasses). Another difference is that pollen grains from C_3 and C_4 grasses are microscopically indistinguishable (Bonnefille and Riollet, 1980) whereas $\delta^{13}C_{wax}$ can differentiate vegetation using C_3 and C_4 photosynthesis. Some plant species produce little pollen while others produce abundant pollen. Likewise, different species of plants produce variable concentrations of leaf waxes (e.g. Vogts et al., 2009), which potentially could lead to a bias in $\delta^{13}C_{wax}$ if large differences in *n*-alkane concentrations exist between C_3 and C_4 species. Both pollen and leaf waxes may be transported by wind and fluvial erosion; however, some pollen types may be selectively dispersed by animal vectors while other types are transported long distances by wind.

During the past 800 ka, our *n*-alkane records suggest interglacial periods in southern East Africa were characterized by relatively wetter conditions with slightly increased contributions of C_3 vegetation. In contrast, glacial periods were characterized by more arid conditions and relatively higher contributions of C_4 vegetation (Figs. 3, 4). Overall, our *n*-alkane records support the pollen

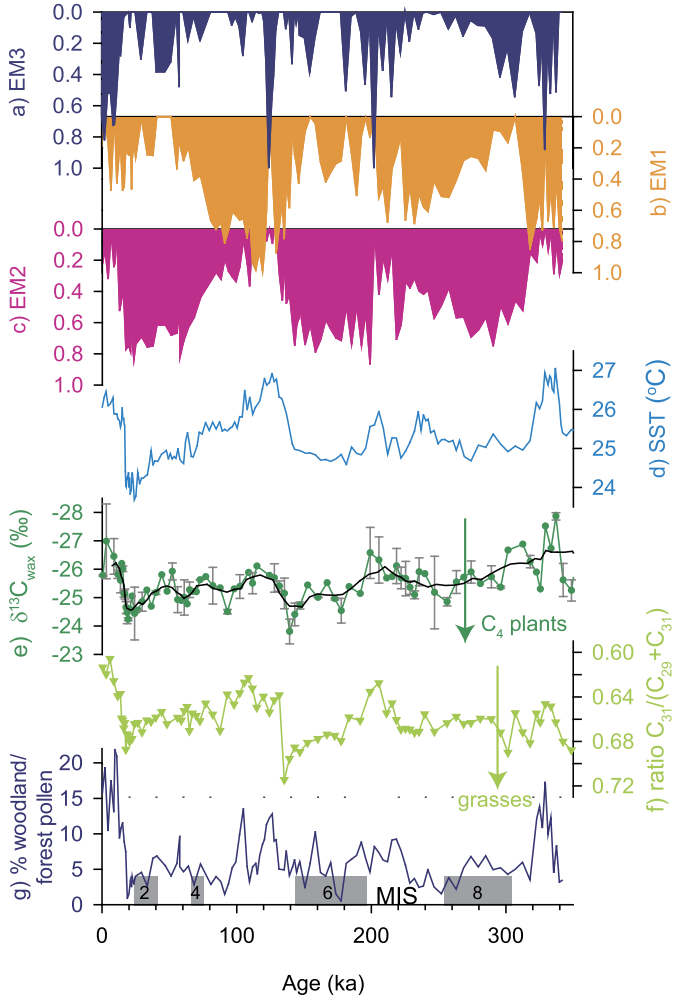

Fig. 4. Comparison between *n*-alkane parameters and pollen assemblage data for the past 350 ka. All pollen data are from Dupont et al. (2011). In a, b and c the results of end-member modeling of the pollen assemblages are displayed (note the reversed *y*-axes). EM3 is plotted in a) and represents a complex assemblage of different biomes with woodland and forest taxa combined with coastal vegetation. EM1 is plotted in b) and represents humid mountainous *Podocarpus* forest and woodland taxa. EM2 is plotted in c) and represents open mountain vegetation dominated by ericaceous scrubs. d) The SST record of MD96-2048 from Caley et al. (2011). e) The carbon isotopic composition of the C_{31} *n*-alkane ($\delta^{13}C_{wax}$). The black line is the 5 point running mean. f) The $C_{31}/(C_{29}+C_{31})$ *n*-alkane ratio. g) The percent of woodland and forest pollen in core MD96-2048. It is notable that woodland/forest pollen is present throughout the entire record. The Marine Isotope Stages (MIS) are indicated by the gray boxes and numbers at the top of the graph. Note the relationships between EM2, SST and the $C_{31}/(C_{29}+C_{31})$ *n*-alkane ratio, supporting that SW Indian Ocean SST is a main control on the vegetation of southern East Africa.

data from the same core, covering the interval from 342 ka to the present (Dupont et al., 2011). MD96-2048 pollen and spore counts were examined by applying a multivariate analysis in the form of an endmember model unmixing procedure to generate a model consisting of three endmembers (EM) (Fig. 4; Dupont et al., 2011). EM1 represents humid mountainous *Podocarpus* forest and woodland taxa, EM2 represents mainly open mountain vegetation dominated by ericaceous scrubs (Ericaceae and Asteroideae) with a swampy component (including Cyperaceae, *Stipularia africana* and *Typha*), and EM3 represents a complex situation of different biomes with woodland and forest taxa combined with coastal vegetation (Dupont et al., 2011). EM1 is the most abundant during periods of intermediate climate between full interglacial and full glacial conditions (MIS 9, 7 and the later part of MIS 5), EM2 is most abundant during full glacial periods (MIS 8, 6 and 2–4) while

EM3 is most abundant during full interglacial stages (MIS 9, 7, 5e and 1) (Fig. 4). Dupont et al. (2011) found that the extent of EM2 (open mountain vegetation) in southern East Africa was driven primarily by SST in this region of the SW Indian Ocean. Here, we also note agreement between the *n*-alkane and SST records (see section 4.4).

To investigate relationships between pollen assemblages and *n*-alkane parameters ($\delta^{13}C_{wax}$ and the $C_{31}/(C_{29}+C_{31})$ ratio), correlations were performed with each of the three endmembers. The $C_{31}/(C_{29}+C_{31})$ ratio was found to exhibit a significant correlation with EM2 ($r = 0.63$, $p < 0.001$) but not with EM1 or EM3. Similarly, the $\delta^{13}C_{wax}$ record, although of lower sampling resolution, also reveals a significant correlation with EM2 ($r = 0.47$, $p < 0.001$). General trends in both records track overall changes in EM2 (Fig. 4); thus it appears that the *n*-alkanes are sensitive to variability in open mountain vegetation. This finding is in agreement with a study of *n*-alkane distributions in modern African vegetation, which found that found savanna herbs, trees and shrubs (i.e. shrubby open mountain vegetation) are dominated by the C_{31} *n*-alkane whereas rain forest vegetation is dominated by the C_{29} *n*-alkane (Vogts et al., 2009).

Although our $\delta^{13}C_{wax}$ record shows similar overall patterns to the $C_{31}/(C_{29}+C_{31})$ ratio, it is relatively more noisy because the analytical error (0.3–0.5‰) is more significant relative to the range (Figs. 3, 4). The maximum overall range of the Limpopo River $\delta^{13}C_{wax}$ record is 4.1‰ but generally glacial–interglacial changes are around 2.5‰. Such glacial–interglacial shifts in $\delta^{13}C_{wax}$ are relatively small in comparison to other East African sites. At Lake Tanganyika (Tierney et al., 2010) and Lake Challa (Sinninghe Damsté et al., 2011), $\delta^{13}C_{wax}$ values vary by approximately 10‰ and 9‰, respectively, between the LGM and the early Holocene. In contrast, a marine core from offshore south western Africa (23°S) exhibits glacial–interglacial shifts in $\delta^{13}C_{wax}$ of ~2.5‰ (Collins et al., 2014). The relatively small range in $\delta^{13}C_{wax}$ is likely because the Limpopo drainage, and also western southern Africa (Collins et al., 2014), did not experience major C_3/C_4 interglacial–glacial shifts like tropical East Africa experienced. The open mountain vegetation assemblage of EM2 includes the families Cyperaceae, Asteraceae, and Poaceae, which contain some C_4 species (Dupont et al., 2011). However, the abundance of Cyperaceae and Asteraceae pollen is low and is likely related to coastal vegetation while Poaceae (includes C_3 and C_4 species) scores only 14% of the taxa on the EM2 assemblage (Dupont et al., 2011). EM3, representing a vegetation complex similar to the present with grasslands present on the interior plateau and forest in the lowlands, also contains Poaceae, which scores about 20% on EM3 (Dupont et al., 2011). Due to the opposing pattern of EM2 dominating during full glacials and EM3 dominating during full interglacials, and the fact that C_4 vegetation is not a dominant component of either end member, it appears that southern East Africa did not experience major glacial/interglacial shifts in C_3 vs. C_4 plant dominance. This may explain why the $\delta^{13}C_{wax}$ record lacks well-defined glacial/interglacial cycles that are better resolved by the $C_{31}/(C_{29}+C_{31})$ ratio.

4.4. SST, orbital forcing and vegetation change in SE Africa

Currently, a strong relationship exists between western Indian Ocean SST and summer rainfall in northern South Africa (Jury et al., 1993; Reason and Mulenga, 1999). A main finding of the pollen analysis of MD96-2048 is that SW Indian Ocean SST was a main control on the extent of open mountain vegetation (EM2) during the past 350 ka (Dupont et al., 2011). We also note a significant negative correlation between the $C_{31}/(C_{29}+C_{31})$ ratio and the SST stack of MD96-2048 ($r = -0.69$, $p < 0.001$), after detrending to remove the long-term trend to lower values, further supporting that SW Indian Ocean SST has been a main control on the vegetation of southern East Africa during the past 800 ka. The $\delta^{13}C_{wax}$ record exhibits a significant but weaker correlation with the SST stack ($r = -0.48$, $p < 0.001$), likely due to the relatively larger noise.

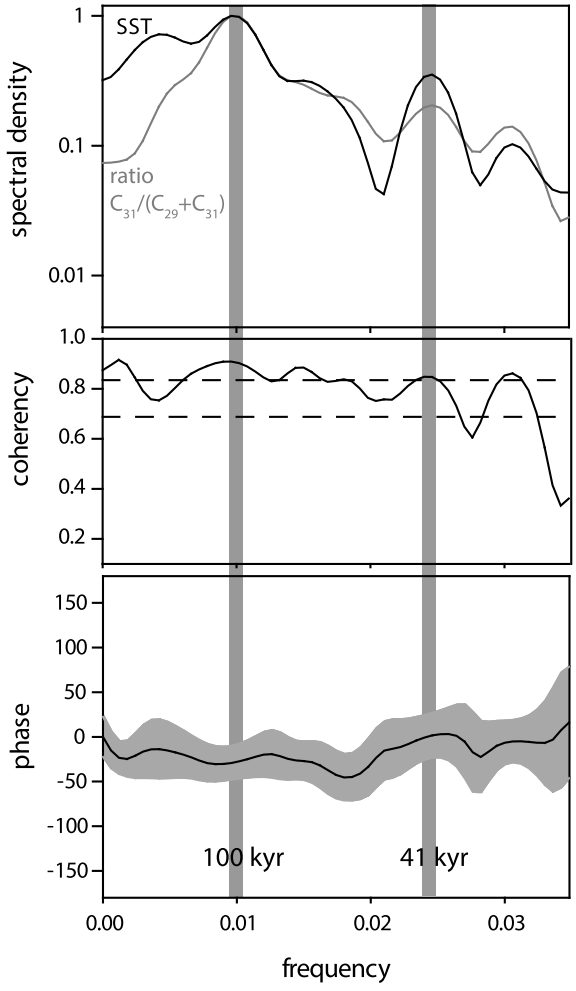

Fig. 5. Cross-spectral analysis between the SST stack (Caley et al., 2011) and the $C_{31}/(C_{29}+C_{31})$ ratio from site MD96-2048. a) Power spectra (log-scale) showing the SST record in black and the $C_{31}/(C_{29}+C_{31})$ ratio in gray, b) coherence with the 80 and 95% confidence intervals indicated by the dashed lines, and c) phase in degrees. Strong 41 kyr cycles are noted in the SST and $C_{31}/(C_{29}+C_{31})$ ratio supporting the role of obliquity in driving SW Indian Ocean SST and vegetation change in southern East Africa.

It was previously found that SST and a qualitative salinity record of MD96-2048 contained strong 100 kyr and 41 kyr cycles (Caley et al., 2011). Likewise, it was found that pollen EM2 (open mountain vegetation) abundances displayed significant power at the 100 kyr and 41 kyr periodicities (Dupont et al., 2011), antiphased with the SST record (e.g. higher proportions of EM2 coincide with lower SST; Fig. 4). While the 100 kyr signal is present in the SST and vegetation records, Caley et al. (2011) found that eccentricity forcing is not significant at site MD96-2048 based on the observation of weak 23 and 19 kyr precession signals, which are modulated by eccentricity, and concluded that high latitude obliquity is the main driver of the Agulhas current system. Spectral analysis of the $C_{31}/(C_{29}+C_{31})$ ratio also reveals strong 100 kyr and 41 kyr cycles (Fig. 5), coherent at the 95% confidence level, further supporting the role of obliquity in driving vegetation change in southern East Africa (Dupont et al., 2011; Caley et al., 2011). We note that the amplitude of the precession signal may be dampened in the pollen and *n*-alkane records due to

a sampling resolution with an average time step of 4.5 kyr. However, a Mg/Ca SST record from this core with a mean time step of 2.5 kyr also failed to yield a precession signal; thus precession likely does not drive SW Indian Ocean SST variability (Caley et al., 2011). Dupont et al. (2011) note that the coring site is at the southern limit of the subtropics and receives seasonal rainfall characteristic of monsoonal climates but not a seasonal wind reversal so a strong influence of precession is not expected in contrast to more equatorial sites. Spectral analysis was conducted on all *n*-alkane parameters but none were found to exhibit a significant precession signal.

4.5. The MBE in southern East Africa

The Mid-Brunhes Event (MBE) is a climate transition that occurred between Marine Isotope Stages (MIS) 12/11 (Jansen et al., 1986; EPICA Community Members, 2004). Antarctic and Southern Ocean records reveal that prior to the MBE interglacials were characterized by higher global ice volume, lower pCO_2 and lower temperatures in comparison to post-MBE interglacials (EPICA Community Members, 2004; Jouzel et al., 2007; Yin, 2013). The MBE is reported in numerous paleoclimate archives, especially from the southern hemisphere. It is debated whether the MBE was a global or regional event as some records, particularly terrestrial records, do not capture the MBE (e.g. Candy and Mcclymont, 2013; Meckler et al., 2012). The vegetation records of MD96-2048 provide insight into the MBE from a subtropical continental setting. In the subsequent discussion we examine two intervals: 800–430 ka (pre-MBE) and 430–0 ka (post-MBE) (Yin, 2013; EPICA Community Members, 2004).

Most *n*-alkane parameters exhibited statistically significant differences at the 95% confidence level between the pre- and post-MBE intervals as determined from a two sample Student's t-test, after first performing an F-test to determine equality of variances. Based on the outcome of the F-test for each *n*-alkane parameter, the appropriate t-test (either assuming unequal or equal variances) was conducted. Only the $\delta^{13}C_{wax}$ record did not show a significant difference between pre- and post-MBE values ($p > 0.05$). We find that the pre-MBE interval is characterized by higher mean ACL and $C_{31}/(C_{29}+C_{31})$ values (Fig. 6). In the EPICA Dome C deuterium isotope (δD) record (not plotted), the MBE transition is not expressed by a change in the mean value of the pre- and post-MBE intervals but rather the post-MBE interval is characterized by a larger amplitude in δD values (EPICA Community Members, 2004). In the EPICA Dome C pCO_2 (Lüthi et al., 2008) and global benthic oxygen isotope (Lisiecki and Raymo, 2005) records, a change in both the mean and amplitude is noted between the pre- and post-MBE intervals (Fig. 6). Most of our records, including the SST stack, also indicate a change in amplitude between the pre- and post-MBE intervals (Fig. 6). We note that we have not excluded MIS 7, recognized as a weak interglacial, or MIS 19, recognized as a strong interglacial, in our analysis as Yin (2013) did, although doing so would result in even more pronounced pre- and post-MBE differences. Overall, our *n*-alkane records indicate that increased shrubby vegetation characterized the pre-MBE interval.

Shifts in the location of oceanic fronts were likely a main cause of differences in the vegetation and climate of southern East Africa on glacial–interglacial timescales as well as in the pre- versus post-MBE intervals. On glacial–interglacial timescales, proxy data indicate that in the SW Indian Ocean, the STF shifted northward during glacials and southward during interglacials of the past 1.5 Ma (Bard and Rickaby, 2009; Caley et al., 2011, 2012). The relative position of the STF exerts an influence on SW Indian Ocean SST in addition to temperature changes associated with insolation-driven glacial–interglacial cycles. Within this context, it is recognized that when the STF reached its most northerly position, such as during MIS 10 and 12, glacial SSTs at MD96-2048 were relatively mild (Caley et al., 2011). In the SW Indian Ocean, an opposite SST response occurs between sites MD96-2048 (26°S) and MD96-2077 (33°S) (Bard and Rickaby, 2009). At site MD96-2077, located near to the present day position of the STF (Fig. 1), extreme northward migration of the STF results in lower SST whereas site MD96-2048 experiences higher SST. This pattern is expected from a northward migration of the STF, which is associated with a contraction of the subtropical gyre and causes the location of the Agulhas retroflection to be shifted to the north and restricted within the Indian Ocean (Sjip and England, 2008).

It appears that shifts in the location of the STF also caused differences in vegetation and SST between the pre- and post-MBE intervals. Our data suggests that in the post-MBE interval both interglacial and glacial periods were characterized by relatively larger inputs of trees and relatively lower SSTs in comparison to the pre-MBE interval. At the Angola Basin, Jansen et al. (1986) report a change from more arid to more humid conditions at 400–350 ka. Yin (2013) examined individual interglacial responses to variable insolation forcing and found that stronger westerlies characterized pre-MBE interglacials, which increased Southern Ocean upwelling and enhanced Antarctic Bottom Water formation. This caused the Antarctic Polar Front (Yin, 2013) and the STF to be located in relatively more northerly positions during the pre-MBE interglacials (Yin, 2015). Relatively higher SST at site MD96-2048 during both glacials and interglacials of the pre-MBE interval support an overall more northerly position of the STF, corroborating the results of Yin (2013).

Interestingly, higher SSTs in the pre-MBE interval are seemingly at odds with the plant leaf wax data suggesting overall increased inputs from grasses (C_{31}), which we interpret as mainly reflecting aridity on glacial–interglacial timescales (see section 4.3). In the modern, higher Indian Ocean SST is associated with increased rainfall in East Africa (Jury et al., 1993; Reason and Mulenga, 1999). However, as noted previously (section 4.2), especially strong glacials/interglacials in the alkane records do not always coincide with strong expression in the SST record, implying a role for other factors in driving vegetation change. A study by Khon et al. (2014) combined paleoecological data and model simulations to examine impacts of rainfall, pCO_2 and temperature on Holocene and LGM (MIS 2) vegetation of the Zambezi River basin. Through different model experiments, they found that precipitation and pCO_2 alone could not account for C_3/C_4 vegetation shifts in the Zambezi basin inferred from $\delta^{13}C_{wax}$. Their study indicates that relatively small temperature changes are important for driving C_3/C_4 shifts with Holocene vegetation controlled by precipitation and temperature, and LGM vegetation mainly controlled by temperature and pCO_2 (Khon et al., 2014). Furthermore, they suggested that temperature influenced the vegetation of southern tropical Africa on long timescales (Khon et al., 2014). Lower pCO_2 and lower temperatures characterize pre-MBE interglacials (EPICA Community Members, 2004; Jouzel et al., 2007; Yin, 2013). Thus, lower temperatures combined with lower pCO_2 perhaps favored grasses (C_{31}) over trees (C_{29}) in the pre-MBE interval despite somewhat higher SST locally.

The strength of the westerlies, and by association the position of the STF, also plays a crucial role in the strength of the Agulhas Current system and leakage (e.g. Caley et al., 2012; Durgadoo et al., 2013). Shifting the STF to the north results in reduced Agulhas leakage (Caley et al., 2012); thus, the overall effect is that reduced Agulhas leakage characterized the pre-MBE interval. The Agulhas leakage transfers heat and salt from the Indian Ocean to the Atlantic Ocean and affects variability in the Atlantic Meridional Overturning Circulation (AMOC) (Caley et al., 2014; Peeters et al., 2004; Weijer et al., 2002), which may explain why the MBE is noted in terrestrial records from Spain (Blain et al., 2012). Increased Agul-

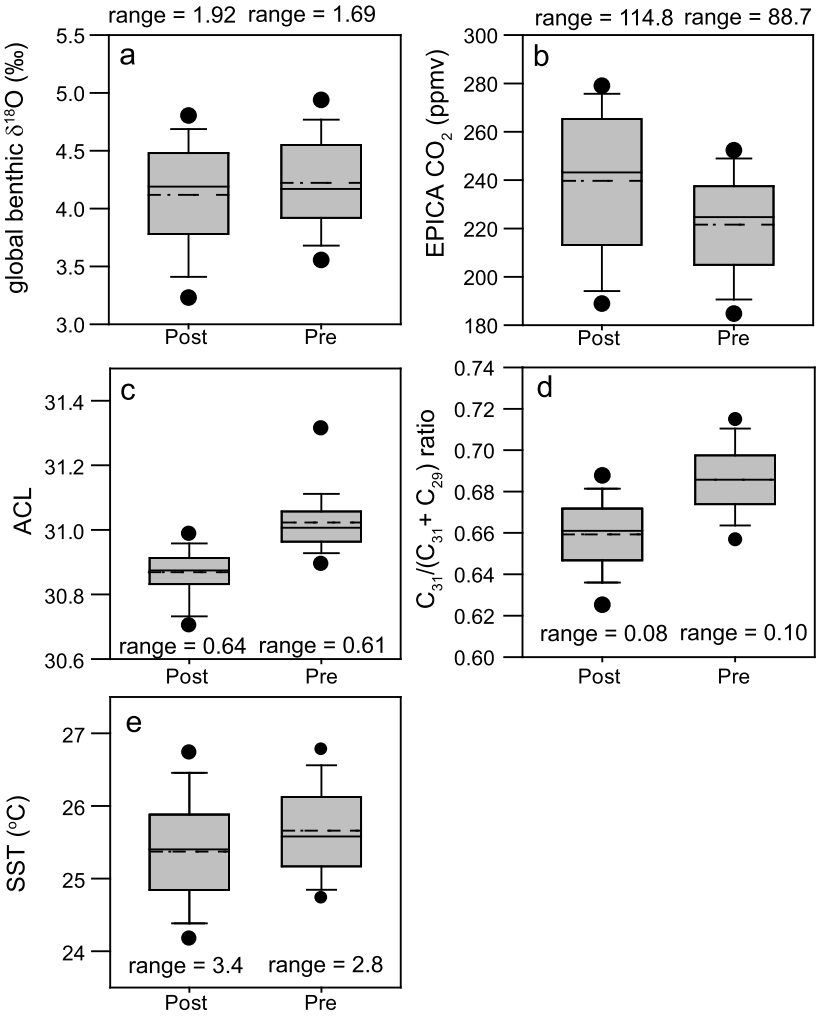

Fig. 6. Box and whisker plots highlighting the differences between pre- and post-MBE intervals in MD96-2048. In all plots the bottom and top of the box indicate the first and third quartiles while the solid line inside the box indicates the median (the second quartile). The dashed line inside of the box indicates the mean, which in a few cases plots on top of the median line. The tips of the whiskers represent the smallest and largest values that are not more than 1.5 times the interquartile range above or below the median. The dots represent the outliers. For all plots, a Student's t-test significant at a 95% confidence level was first performed to test the null hypothesis that the means of the pre- and post-MBE intervals are the same; for all parameters the null hypothesis was rejected. a) The global benthic LR04 oxygen isotope stack (Lisiecki and Raymo, 2005). b) Carbon dioxide (CO_2) data from the EPICA Dome C ice core (Lüthi et al., 2008) in units of parts per million by volume (ppmv). c) MD96-2048 *n*-alkane average chain length (ACL) values. d) MD96-2048 $C_{31}/(C_{29}+C_{31})$ *n*-alkane ratio. e) SST stack at site MD96-2048. Data from Caley et al. (2011). The range of the data for the pre- and post-MBE intervals is indicated on the plots.

has leakage during post-MBE glacials could also explain why the ODP Site 1082 (Fig. 1) planktonic $\delta^{18}O$ record shows higher glacial SSTs in the post-MBE interval (Jahn et al., 2003). Lower SSTs at site MD96-2048 in conjunction with higher SSTs at ODP Site 1082 are consistent with increased Agulhas leakage during post-MBE glacials. Outside of the southern high latitudes and locations that directly fall under the influence of the Antarctic Polar Front or the STF, regions that are sensitive to AMOC variability may be well suited for recording the MBE.

4.6. Variability in mid- to late-Pleistocene African landscapes

The African landscape is recognized as important to hominin development and therefore understanding the mechanisms driving vegetation dynamics on a variety of timescales is of interest. Pleistocene vegetation records reveal highly variable conditions across the African continent. A compilation of West African marine pollen records indicates that despite strong fluctuations, the latitudinal arrangement of biomes has been conserved through the past three or four climate cycles (Dupont, 2011). There is some tendency toward increased forest vegetation during interglacials while during glacials an equatorward savanna shift into the modern rain forest area is suggested (Dupont, 2011). At elevated areas open mountainous scrubland was widespread during the glacials, alternating with phases in which mountain forests expanded, with *Podocarpus* maxima falling mostly between the extremes of full glacials or full interglacials (Dupont, 2011).

At Lake Malawi (11°S) multi-proxy records including pollen indicate a "megadrought", occurring during MIS 6 and persisting for 18,000 yr (Lane et al., 2013; Beuning et al., 2011; Scholz et al., 2007; Cohen et al., 2007). During the megadrought, the volume of water in Lake Malawi was reduced by at least 95% (Scholz et al., 2007) and grass-dominated vegetation was limited, implying extreme aridity and suggesting conditions that would have been inhospitable to humans in the region (Beuning et al., 2011). Our Limpopo basin vegetation records contrast significantly as we find no evidence of the megadrought (Fig. 4) suggesting that the extreme aridity was confined to more tropical sites. In MD96-2048, the proportion of EM1, reflecting mainly humid mountainous *Podocarpus* forest, is relatively high at this time (Dupont et al., 2011) while no significant changes in the $C_{31}/(C_{29}+C_{31})$ ratio or $\delta^{13}C_{wax}$ are observed (Fig. 4). Although glacial–interglacial

changes in the vegetation of southern East Africa are observed, notably woodland/forest pollen persists throughout the entire record (Dupont et al., 2011) (Fig. 4). The continued presence of trees on the landscape indicates substantially less variability in the vegetation of southern East Africa in comparison to the Lake Malawi region. Beuning et al. (2011) noted consistency between Lake Malawi and West African pollen records (Angola and Congo basins) and suggested that large scale vegetation changes were not controlled by SST but rather by changes in Hadley circulation or ITCZ position, which would be sensitive to precession. However, we find that SW Indian Ocean SST variability, driven by obliquity, exerted the main control on southern East African vegetation. Dupont (2011) concluded that while the representation of tropical rain forest fluctuated with summer insolation and precession, the subtropical biomes showed more obliquity variability or followed the pattern of glacial and interglacials.

The emerging picture is that Pleistocene environments of the southern African continent were more stable in contrast to those of tropical Africa. In recent years the southern African continent has received an increasing amount of attention as a region critical to hominin evolution and the appearance of modern behavior (Compton, 2011). Our results support the hypothesis that the southern African continent provided suitable living environments for hominins and fauna throughout the Pleistocene, which may have been especially important at times when tropical Eastern Africa experienced extreme aridity.

5. Conclusions

Paired analyses of plant leaf waxes and pollen assemblages reveal insights into Pleistocene vegetation change in southern East Africa. We find that while the Limpopo River basin did not experience major glacial–interglacial changes in C_3 vs. C_4 vegetation, *n*-alkanes chain lengths are sensitive to varying inputs of open mountain vegetation, which is closely tied to SW Indian Ocean SST. In turn, the SST of the SW Indian Ocean largely reflects changes in high-latitude obliquity. Our leaf wax records indicate a clear response of the southern East African vegetation to glacial–interglacial climate variability as well as to the MBE. Differences between pre- and post-MBE vegetation and climate of southern East Africa are attributed to shifts in the position of the STF, and associated changes in the strength of the Agulhas leakage and AMOC may have been important for transmitting the MBE outside of the southern high latitudes. Overall, our vegetation records indicate that while glacial–interglacial changes in vegetation assemblages occurred, and a long-term shift took place over the past 800 ka, in general landscapes of subtropical southern East Africa were relatively stable compared to those of tropical East Africa. The relatively stable Pleistocene environments of southern East Africa may have provided an important refuge for early hominins and fauna at times when inhospitable conditions occurred in tropical East Africa.

Acknowledgements

We thank Michiel Kienhuis, Monique Verweij, Marianne Baas, Ellen Hopmans and Jort Ossebaar for analytical assistance. Qiuzhen Yin is especially acknowledged for examining her model output from Yin (2013) to investigate the movement of the subtropical front during pre- and post-MBE interglacials. We are grateful to Dr. Jessica Tierney and an anonymous reviewer for insightful comments that helped clarify and improve the manuscript. The Netherlands Organization for Scientific Research (NWO) is thanked for financial support through a VICI grant to S. Schouten. Core MD96-2048 was collected during the MOZAPHARE cruise of the RV Marion Dufresne, supported by the French agencies Ministère de l'Education Nationale de la Recherche et de la Technologie, Centre National de la Recherche Scientifique (CNRS), and Institut Paul Emile Victor (IPEV). This work was supported by the "Laboratoire d'Excellence" LabexMER (ANR-10-LABX-19) and co-funded by a grant from the French government under the program "Investissements d'Avenir", and by a grant from the Regional Council of Brittany (SAD programme). T.C. is supported by CNRS-INSU.

References

Bard, E., Rickaby, R.E., 2009. Migration of the subtropical front as a modulator of glacial climate. Nature 460, 380–383.
Beuning, K.R., Zimmerman, K.A., Ivory, S.J., Cohen, A.S., 2011. Vegetation response to glacial–interglacial climate variability near Lake Malawi in the southern African tropics. Palaeogeogr. Palaeoclimatol. Palaeoecol. 303, 81–92.
Blain, H.A., Cuenca-Bescos, G., Lozano-Fernandez, I., Lopez-Garcia, J.M., Olle, A., Rosell, J., Rodriguez, J., 2012. Investigating the Mid-Brunhes Event in the Spanish terrestrial sequence. Geology 40, 1051–1054.
Bonnefille, R., Riollet, G., 1980. Pollen des savanes d'Afrique orientale. Éditions du Centre National de la Recherche Scientifique, Paris. 140 pp., 113 plates.
Bush, R.T., McInerney, F.A., 2015. Influence of temperature and C_4 abundance on *n*-alkane chain length distributions across the central USA. Org. Geochem. 79, 65–73.
Caley, T., Kim, J.H., Malaize, B., Giraudeau, J., Laepple, T., Caillon, N., Charlier, K., Rebaubier, H., Rossignol, L., Castañeda, I., Schouten, S., Sinninghe Damste, J.S., 2011. High-latitude obliquity as a dominant forcing in the Agulhas current system. Clim. Past 7, 1285–1296.
Caley, T., Giraudeau, J., Malaizé, B., Rossignol, L., Pierre, C., 2012. Agulhas leakage as a key process in the modes of Quaternary climate changes. Proc. Natl. Acad. Sci. USA 109, 6835–6839.
Caley, T., Peeters, F.J., Biastoch, A., Rossignol, L., Sebille, E., Durgadoo, J., Malaizé, B., Giradeau, J., Arthur, K., Zahn, R., 2014. Quantitative estimate of the paleo-Agulhas leakage. Geophys. Res. Lett. 41, 1238–1246.
Candy, I., McClymont, E.L., 2013. Interglacial intensity in the North Atlantic over the last 800 000 years: investigating the complexity of the mid-Brunhes Event. J. Quat. Sci. 28, 343–348.
Castañeda, I.S., Mulitza, S., Schefuss, E., dos Santos, R.A.L., Sinninghe Damsté, J.S., Schouten, S., 2009a. Wet phases in the Sahara/Sahel region and human migration patterns in North Africa. Proc. Natl. Acad. Sci. USA 106, 20159–20163.
Castañeda, I.S., Werne, J.P., Johnson, T.C., Filley, T.R., 2009b. Late Quaternary vegetation history of southeast Africa: the molecular isotopic record from Lake Malawi. Palaeogeogr. Palaeoclimatol. Palaeoecol. 275, 100–112.
Castañeda, I.S., Schouten, S., Pätzold, J., Lucassen, F., Kasemann, S., Kuhlmann, H., Schefuß, E., 2016. Hydroclimate variability in the Nile River Basin during the past 28,000 years. Earth Planet. Sci. Lett. 438, 47–56.
Cohen, A.S., Stone, J.R., Beuning, K.R., Park, L.E., Reinthal, P.N., Dettman, D., Scholz, C.A., Johnson, T.C., King, J.W., Talbot, M.R., Brown, E.T., 2007. Ecological consequences of early Late Pleistocene megadroughts in tropical Africa. Proc. Natl. Acad. Sci. USA 104, 16422–16427.
Collins, J.A., Schefuß, E., Govin, A., Mulitza, S., Tiedemann, R., 2014. Insolation and glacial–interglacial control on southwestern African hydroclimate over the past 140 000 years. Earth Planet. Sci. Lett. 398, 1–10.
Collister, J.W., Rieley, G., Stern, B., Eglinton, G., Fry, B., 1994. Compound-specific delta-C-13 analyses of leaf lipids from plants with differing carbon-dioxide metabolisms. Org. Geochem. 21, 619–627.
Compton, J.S., 2011. Pleistocene sea-level fluctuations and human evolution on the southern coastal plain of South Africa. Quat. Sci. Rev. 30 (5–6), 506–527.
deMenocal, P.B., 2004. African climate change and faunal evolution during the Pliocene–Pleistocene. Earth Planet. Sci. Lett. 220, 3–24.
Diefendorf, A.F., Mueller, K.E., Wing, S.L., Freeman, K.H., 2010. Global patterns in leaf ^{13}C discrimination and implications for studies of past and future climate. Proc. Natl. Acad. Sci. USA 107, 5738–5743.
Dupont, L., 2011. Orbital scale vegetation change in Africa. Quat. Sci. Rev. 30, 3589–3602.
Dupont, L.M., Caley, T., Kim, J.H., Castañeda, I., Malaizé, B., Giraudeau, J., 2011. Glacial–interglacial vegetation dynamics in South Eastern Africa coupled to sea surface temperature variations in the Western Indian Ocean. Clim. Past 7, 1209–1224.
Dupont, L.M., Rommerskirchen, F., Mollenhauer, G., Schefuß, E., 2013. Miocene to Pliocene changes in South African hydrology and vegetation in relation to the expansion of C_4 plants. Earth Planet. Sci. Lett. 375, 408–417.
Durgadoo, J.V., Loveday, B.R., Reason, C.J., Penven, P., Biastoch, A., 2013. Agulhas leakage predominantly responds to the Southern Hemisphere westerlies. J. Phys. Oceanogr. 43, 2113–2131.
Eglinton, G., Hamilton, R.J., 1967. Leaf epicuticular waxes. Science 156, 1322–1335.
EPICA Community Members, 2004. Eight glacial cycles from an Antarctic ice core. Nature 429, 623–628.

Feakins, S.J., 2013. Pollen-corrected leaf wax D/H reconstructions of northeast African hydrological changes during the late Miocene. Palaeogeogr. Palaeoclimatol. Palaeoecol. 374, 62–71.
Feakins, S.J., Sessions, A.L., 2010. Crassulacean acid metabolism influences D/H ratio of leaf wax in succulent plants. Org. Geochem. 41, 1269–1276.
Hoetzel, S., Dupont, L., Schefuß, E., Rommerskirchen, F., Wefer, G., 2013. The role of fire in Miocene to Pliocene C_4 grassland and ecosystem evolution. Nat. Geosci. 6, 1027–1030.
Horikawa, K., Murayama, M., Minagawa, M., Kato, Y., Sagawa, T., 2010. Latitudinal and downcore (0–750 ka) changes in *n*-alkane chain lengths in the eastern equatorial Pacific. Quat. Res. 73, 573–582.
Huang, Y., Shuman, B., Wang, Y., Webb III, T., Grimm, E.C., Jacobson, J., 2006. Climatic and environmental controls on the variation of C_3 and C_4 plant abundances in central Florida for the past 62,000 years. Palaeogeogr. Palaeoclimatol. Palaeoecol. 237, 428–435.
Hughen, K.A., Eglinton, T.I., Xu, L., Makou, M., 2004. Abrupt tropical vegetation response to rapid climate changes. Science 304, 1955–1959.
Jahn, B., Donner, B., Müller, P.J., Röhl, U., Schneider, R.R., Wefer, G., 2003. Pleistocene variations in dust input and marine productivity in the northern Benguela Current: evidence of evolution of global glacial–interglacial cycles. Palaeogeogr. Palaeoclimatol. Palaeoecol. 193, 515–533.
Jansen, J.H.F., Kuijpers, A., Troelstra, S.R., 1986. A Mid-Brunhes Climatic Event – long-term changes in global atmosphere and ocean circulation. Science 232, 619–622.
Jouzel, J., Masson-Delmotte, V., Cattani, O., Dreyfus, G., Falourd, S., Hoffmann, G., Wolff, E.W., 2007. Orbital and millennial Antarctic climate variability over the past 800,000 years. Science 317 (5839), 793–796.
Jury, M.R., Valentine, H.R., Lutjeharms, J.R., 1993. Influence of the Agulhas Current on summer rainfall along the southeast coast of South Africa. J. Appl. Meteorol. 32, 1282–1287.
Just, J., Schefuß, E., Kuhlmann, H., Stuut, J.B.W., Pätzold, J., 2014. Climate induced sub-basin source-area shifts of Zambezi River sediments over the past 17 ka. Palaeogeogr. Palaeoclimatol. Palaeoecol. 410, 190–199.
Khon, V.C., Wang, Y.V., Krebs-Kanzow, U., Kaplan, J.O., Schneider, R.R., Schneider, B., 2014. Climate and CO_2 effects on the vegetation of southern tropical Africa over the last 37,000 years. Earth Planet. Sci. Lett. 403, 407–417.
Lane, C.S., Chorn, B.T., Johnson, T.C., 2013. Ash from the Toba supereruption in Lake Malawi shows no volcanic winter in East Africa at 75 ka. Proc. Natl. Acad. Sci. USA 110, 8025–8029.
Lang, N., Wolff, E.W., 2011. Interglacial and glacial variability from the last 800 ka in marine, ice and terrestrial archives. Clim. Past 7 (2), 361–380.
Lisiecki, L.E., Raymo, M.E., 2005. A Pliocene–Pleistocene stack of 57 globally distributed benthic delta O-18 records. Paleoceanography 20.
Lüthi, D., Le Floch, M., Bereiter, B., Blunier, T., Barnola, J.M., Siegenthaler, U., et al., 2008. High-resolution carbon dioxide concentration record 650,000–800,000 years before present. Nature 453, 379–382.
Martin, A.K., 1981. Evolution of the Agulhas Current and its palaeo-ecological implications. South Afr. J. Sci. 77, 547–554.
Meckler, A., Clarkson, M., Cobb, K., Sodemann, H., Adkins, J., 2012. Interglacial hydroclimate in the tropical West Pacific through the Late Pleistocene. Science 336, 1301–1304.
Past Interglacials Working Group of PAGES, 2016. Interglacials of the last 800,000 years. Rev. Geophys. 54, 162–219.
Peeters, F.J., Acheson, R., Brummer, G.J.A., De Ruijter, W.P., Schneider, R.R., Ganssen, G.M., Ufkes, E., Kroon, D., 2004. Vigorous exchange between the Indian and Atlantic oceans at the end of the past five glacial periods. Nature 430, 661–665.
Ponton, C., West, A.J., Feakins, S.J., Galy, V., 2014. Leaf wax biomarkers in transit record river catchment composition. Geophys. Res. Lett. 41, 6420–6427.
Poynter, J.G., Farrimond, P., Robinson, N., Eglinton, G., 1989. Aeolian-derived higher plant lipids in the marine sedimentary record: links with palaeoclimate. In: Leinen, M., Sarnthein, M. (Eds.), Paleoclimatology and Paleometeorology: Modern and Past Patterns of Global Atmospheric Transport. Kluwer, Dordrecht, pp. 435–462.
Reason, C.J.C., Mulenga, H., 1999. Relationships between South African rainfall and SST anomalies in the Southwest Indian Ocean. Int. J. Climatol. 19, 1651–1673.
Rommerskirchen, F., Eglinton, G., Dupont, L., Guntner, U., Wenzel, C., Rullkotter, J., 2003. A north to south transect of Holocene southeast Atlantic continental margin sediments: relationship between aerosol transport and compound-specific $\delta^{13}C$ land plant biomarker and pollen records. Geochem. Geophys. Geosyst. 4.
Rommerskirchen, F., Eglinton, G., Dupont, L., Rullkoetter, J., 2006. Glacial/interglacial changes in southern Africa: compound-specific delta C-13 land plant biomarker and pollen records from southeast Atlantic continental margin sediments. Geochem. Geophys. Geosyst. 7.
Schefuß, E., Schouten, S., Jansen, J.H.F., Sinninghe Damsté, J.S., 2003. African vegetation controlled by tropical sea surface temperatures in the mid-Pleistocene period. Nature 422, 418–421.
Schefuß, E., Kuhlmann, H., Mollenhauer, G., Prange, M., Pätzold, J., 2011. Forcing of wet phases in southeast Africa over the past 17,000 years. Nature 480, 509–512.
Scholz, C.A., Johnson, T.C., Cohen, A.S., King, J.W., Peck, J.A., Overpeck, J.T., Talbot, M.R., Brown, E.T., Kalindekafe, L., Amoako, P.Y.O., Lyons, R.P., Shanahan, T.M., Castañeda, I.S., Heil, C.W., Forman, S.L., McHargue, L.R., Beuning, K.R., Gomez, J., Pierson, J., 2007. East African megadroughts between 135 and 75 thousand years ago and bearing on early-modern human origins. Proc. Natl. Acad. Sci. USA 104, 16416–16421.
Schulz, H., Lückge, A., Emeis, K.C., Mackensen, A., 2011. Variability of Holocene to Late Pleistocene Zambezi riverine sedimentation at the upper continental slope off Mozambique, 15–21 S. Mar. Geol. 286, 21–34.
Sinninghe Damsté, J.S., Verschuren, D., Ossebaar, J., Blokker, J., van Houten, R., van der Meer, M.T., Schouten, S., 2011. A 25,000-year record of climate-induced changes in lowland vegetation of eastern equatorial Africa revealed by the stable carbon-isotopic composition of fossil plant leaf waxes. Earth Planet. Sci. Lett. 302, 236–246.
Tierney, J.E., Russell, J.M., Huang, Y., 2010. A molecular perspective on Late Quaternary climate and vegetation change in the Lake Tanganyika basin, East Africa. Quat. Sci. Rev. 29, 787–800.
Trauth, M.H., Larrasoaña, J.C., Mudelsee, M., 2009. Trends, rhythms and events in Plio-Pleistocene African climate. Quat. Sci. Rev. 28, 399–411.
Tyson, P.D., Preston-Whyte, R.A., 2000. The Weather and Climate of Southern Africa. Oxford University Press, Cape Town.
van der Lubbe, H.J.L., Tjallingii, R., Prins, M.A., Brummer, G.J.A., Jung, S.J., Kroon, D., Schneider, R.R., 2014. Sedimentation patterns off the Zambezi River over the last 20,000 years. Mar. Geol. 355, 189–201.
van der Lubbe, H.J.L., Frank, M., Tjallingii, R., Schneider, R.R., 2016. Neodymium isotope constraints on provenance, dispersal, and climate-driven supply of Zambezi sediments along the Mozambique Margin during the past ~45,000 years. Geochem. Geophys. Geosyst. 17, 181–198.
Vogts, A., Moossen, H., Rommerskirchen, F., Rullkötter, J., 2009. Distribution patterns and stable carbon isotopic composition of alkanes and alkan-1-ols from plant waxes of African rain forest and savanna C_3 species. Org. Geochem. 40, 1037–1054.
Vogts, A., Schefuß, E., Badewien, T., Rullkötter, J., 2012. *n*-Alkane parameters from a deep sea sediment transect off southwest Africa reflect continental vegetation and climate conditions. Org. Geochem. 47, 109–119.
Weijer, W., De Ruijter, W.P., Sterl, A., Drijfhout, S.S., 2002. Response of the Atlantic overturning circulation to South Atlantic sources of buoyancy. Glob. Planet. Change 34 (3), 293–311.
Weijers, J.W.H., Schouten, S., van den Donker, J.C., Hopmans, E.C., Sinninghe Damsté, J.S., 2007. Environmental controls on bacterial tetraether membrane lipid distribution in soils. Geochim. Cosmochim. Acta 71 (3), 703–713.
White, F., 1983. The Vegetation of Africa. A Descriptive Memoir to Accompany the UNESCO/AETFAT/UNSO Vegetation Map of Africa. Nat. Resour. Res., vol. 20. UNESCO, Paris.
Yin, Q., 2013. Insolation-induced mid-Brunhes transition in Southern Ocean ventilation and deep-ocean temperature. Nature 494 (7436), 222–225.
Yin, Q., 2015. Personal communication.